ON THE USE OF FDTD FOR HIRF VALIDATION AND CERTIFICATION

G. G. Gutiérrez[1], S. F. Romero[2], J. Alvarez[3], S. G. Garcia[4, *], and E. P. Gil[5]

[1]EMC & MW Department, AIRBUS MILITARY, Getafe, Spain

[2]EMC — Aircraft Test Group, INTA, Torrejón de Ardoz, Spain

[3]EMC/EMI Department, Cassidian, Getafe, Spain

[4]University of Granada, Granada, Spain

[5]EMC & MW Department, AIRBUS MILITARY, Getafe, Spain

Abstract—Preparing the 3D-geometry models to perform electromagnetic compatibility (EMC) numerical simulations can be tedious and time consuming. Furthermore, the need to include the test setup in the models, in order to validate the software, by comparing the numerical results with the measured data, may lead to unwieldy simulation models with often unaffordable computational costs. In this paper, we illustrate a procedure to optimize and simplify the modeling process, together with guidelines for achieving the most unfavorable case in the simulation of EMC problems, as required for a certification process. A test case from the European FP7 HIRF-SE (High-Intensity Radiated Field Synthetic Environment) project is analyzed in this paper as an example of how to identify the unnecessary elements for the simulation, while retaining the essential physics of the problem.

1. INTRODUCTION

Numerical techniques have been broadly employed in EMC assessment (e.g., [1–4]). Among them Finite Difference Time Domain (FDTD), has become an invaluable technique, since it is able to model both the interior and the exterior problem by taking into account any material and geometrical detail. The classical FDTD method employs a second-order finite centered approximation to the space and time derivatives

---

in order to solve Maxwell's curl equations in the time domain [5–8]. It employs a staggered orthogonal cubic spatial grid based on the Yee unit-cell, on which the time evolution of the fields is found by a leap-frog algorithm. The materials are modeled by specifying their constitutive parameters at each grid point, in homogeneous regions. Open problems are simulated by placing truncation conditions, such as Perfectly Matched Layers (PML), in the terminating planes of the grid [9]. The numerical scheme must fulfill the stability criterion on the time step given by the Courant-Friedrichs-Lewy (CFL) condition [6], so that the smaller the cell size, the shorter the time step is required and the longer the computation time is to reach a given physical time.

Good comparisons between FDTD simulations and EMC measurements often require the whole test setup to be modeled together with the equipment under test (EUT). For instance, in order to catch all the significant geometrical details of a typical aircraft, for problems below 1 GHz, cells sizes are usually in the range of mm to cm. Simulations of several hundreds of Mcells are often required, with computational times in the range of several days in modern supercomputers (some microseconds may be needed to predict the low-frequency interior resonances, especially under 1 MHz).

Thus, a key point in EMC simulations of aircrafts, resides in the reduction on the meshing details, to keep CPU times affordable for engineering purposes. The modeler must find some trade-off to keep all the details electromagnetically relevant, discarding the unnecessary ones. For instance, pieces that make the contacts which ensure the current flow between different zones of the structure must be guaranteed to be correctly modeled so as to prevent severe errors.

The European FP7 HIRF-SE project [10] is intended to provide the aeronautics industry with a Synthetic Environment integrated by a numerical simulation toolset (FDTD, Method of Moments, Finite elements, etc.), in order to predict the coupling of High-Intensity Radiated Field (HIRF) into the cable links within an aircraft. The frequency spectrum of HIRF threats ranges from 10 kHz to 40 GHz. Below 400 MHz, the dominant effect in the RF energy comes from the excitation of airframe resonances. Above 100 MHz, the penetration of the field into the equipment bays via gaps, seams, RF transparent materials and apertures in the airframe structure and equipment enclosures, becomes more and more the significant coupling mechanism.

In this paper, we will describe the simulation of a general object (hereafter called GO31), which has been proposed under the HIRF-SE project to serve as a test case of several numerical solvers. The experimental data has been gathered using the commonly used Low-

Level Swept Current (LLSC) test method [11, 12] (from 0.5 MHz up to 400 MHz).

The numerical modeling of this object will be employed to describe general strategies for its simulation with FDTD, optimization of the modeling process and definition of guidelines for reaching the worst possible level in order to use the simulation in a certification process.

2. FDTD FOR HIRF SIMULATION

2.1. GO31 Test Case Description

Antecedents exist for applying FDTD to HIRF problems [13]. In this paper, we illustrate the application of a FDTD MPI-parallel solver [7, 8] by the Univ. of Granada in Spain (UGRFDTD [14][†]) to the GO31 test case, which consists of a real onboard shielded harness over a ground plane. This harness is installed on the aerial refueling boom system of the A330 multi-role tanker transport aircraft, developed by Airbus Military [15].

The cable consists of four shielded twisted pairs with a common overall screen. The harness length is 6.3 m and the outer diameter is 15 mm. There are six outer-shield ground connections distributed along the cable. The cable is connected to known impedances at both ends. The harness is perfectly connected to two metal boxes that represent the aircraft's real equipments. The cable is suspended 50 mm over the ground plane. A 0.5-mm-thick aluminum ground plane of 1 m × 3 m was located in the middle of the platform, supported by 4 polystyrene blocks 0.96 m high.

Measurements of LLSC according to SAE ARP 5583 [12] were performed by the National Institute for Aerospace Technology (INTA) of Spain in their open-area test-site facility (see Fig. 1). The setup consists of a concrete platform 50 m × 50 m, illuminated by three different antennas to cover the frequency range from 2 MHz to 400 MHz and both polarizations: between 2 MHz and 30 MHz, a horizontal dipole 15.2 m long and a vertical dipole 6.2 m long, and between 27 MHz and 400 MHz, a biconilog log-periodic bow-tie antenna model 3143 manufactured by EMCO. The antennas were placed 6 m away from the EUT.

Before the test, the electric field level at the location of the EUT in its absence was measured in order to determine the calibration field. All currents measured have been normalized by this calibration field, refered as transfer functions.

[†] UGRFDTD has been thoroughly validated with experimental data and with academic and commercial time/frequency domain solvers under the HIRF-SE project [10].

Figure 1. Experimental setup with the EMCO antenna at the INTA open-area test-site facility.
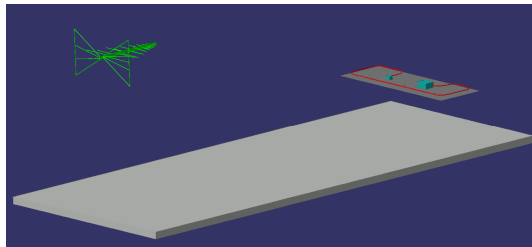
Figure 2. CAD model of the EMCO antenna test setup.

In this paper, we focus only on the tuning analysis for the EMCO antenna with horizontal polarization. The normalized currents determined for the two probes located at a distance of 50 mm of both equipments (big and small boxes) are used for the comparisons. These currents injected into the equipment are the required figures for certification and equipment specification in aerospace [12].

2.2. Initial Approach to a Numerical Model

As an initial FDTD model of the experimental setup, we have tried to model each particular detail (Fig. 2). Though there is a number of cable equivalent models for FDTD [16, 17] (also included in the UGRFDTD solver), in this paper we show the results only for a staircased meshed version of the cable, since no computational over-load is needed, while finding good agreement with the measurements. A comparison of thin and meshed modeling of the cables in FDTD is left for a forthcoming study.

For the platform floor, a lossy dielectric is used, truncated by a
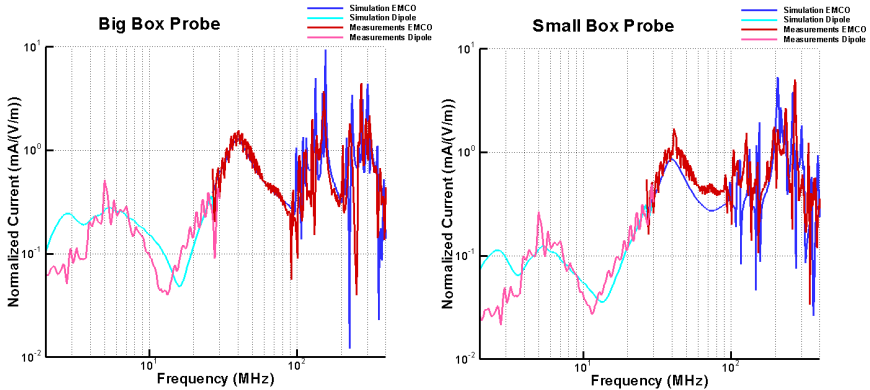
Figure 3. GO31 test case. Comparison between measurements and simulation for the configuration with EMCO and Dipole antennas (horizontal polarization).

lower PML boundary condition, with a conductivity of 5 mS/m and a relative permittivity of 10. The external geometry of the EMCO antenna has been modeled and excited with a Gaussian pulse whose frequency spectrum covers the range of interest. The ground plane and the two boxes at each end of the harness have been modeled with metallic surfaces. The harness consists of a cylindrical tube with six bonding strips. All the surfaces have been considered to be PEC since electromagnetic diffusion in such a highly conductive over braid can be neglected.

An FDTD problem with 630 Mcells ($1511 \times 653 \times 636$), uniformly meshed with cells of 6.5 mm per side, and a time step of 0.01 ns, is yielded. This problem requires around 32 GB of memory and approximately 6.15 sec of CPU time to simulate 1 ns. of physical time in a 512-core Xeon X5650 cluster (UGRFDTD scales around 20 Mcells/sec/core in MPI clusters). Typically a physical time of 3 µs is enough for convergence (around 5 hours of CPU time).

In the same manner that in the test procedure, the computed currents are normalized by the incident field previously computed in absence of the EUT. The curves that show the comparison between measured data and numerical results are shown in Fig. 3. Ampere loops around the cable endings close to the equipments have been used to calculate the bulk current induced in the cable, by integrating the magnetic field along the loop path. As can be seen in the figure, the agreement between measurements and simulations is excellent except at the lowest frequencies, where some minor deviations are found.
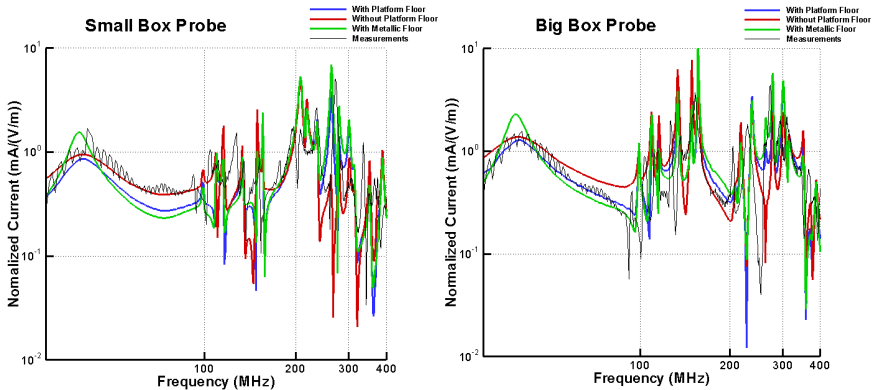
Figure 4. Comparison with/without platform floor.

3. SENSITIVITY ANALYSIS AND MODEL TUNING

In this section, we compute the sensitivity of the results to variations of the model in order to estimate the expected differences due to a simplification of the numerical approach, like the substitution of the actual antenna by a plane-wave source, or the impact of the uncertainty on different parameters such as the probe location.

3.1. Platform Floor Removal

Considering the platform floor in the simulations, even though it affects the incident field, may not have an effect on the estimation of the induced current transfer functions since they are normalized with respect to the calibration field. The need to introduce the platform floor in the simulations has been analyzed by the computation of the transfer functions with and without the platform floor, and considering different materials for the platform floor. The comparison between the different cases are shown in Fig. 4.

Two different platform floors has been simulated, one of them made of concrete and the other one modeled as PEC (Perfect Electric Conductor). The results with and without a platform floor are very similar, since, as mentioned, the normalization by the calibration field minimizes this effect and the contribution of the wave bouncing between the platform floor and the ground plane has no influence. Hence, the platform floor can be removed from the numerical test setup, leading to reductions in the computational cost by a factor 1.2.

3.2. Antenna Replacement by a Plane-wave Source

According to the standards [12], the distance between the antenna and the EUT should be at least 1.5 times the length of the EUT in order to produce less than 3 or 4 dB of variation over the length of the EUT. The field homogeneity was measured during the tests and a variation of less than 3 dB was found at a distance of 6 m.

The far–field limit of the antenna can be estimated by requiring the fulfillment of both, the fundamental limit for radiation $r \geq \frac{\lambda}{2\pi}$, and the Fraunhofer condition $r \geq \frac{2D^2}{\lambda}$, where r is the minimum distance between the antenna and the EUT, D is the largest dimension of the antenna and λ the wavelength [18]. For high frequencies (electrically medium/large antenna), the Fraunhofer far-field condition dominates

$$r \geq \frac{2 \times 1.47^2}{0.75} \cong 6\,\mathrm{m} \tag{1}$$

however, for electrically-small antennas (low frequency) the fundamental limit is dominant and requires

$$r \geq \frac{\lambda}{2\pi} \cong 1.6\,\mathrm{m} \tag{2}$$

Therefore, the antenna can be replaced in the numerical setup, by a plane-wave Huygens total-field/scattered-field surface [6], surrounding the EUT (harness plus boxes above their ground plane), one cell away from the PML absorbing boundary conditions. We now require a $(307 \times 615 \times 206)$ region (39 Mcells), leading to a reduction in the computational cost of a factor 16, both in memory and in CPU time.

The results over the whole frequency range from 2 MHz up to 400 MHz (dipole and EMCO antenna) can be seen in Fig. 5,
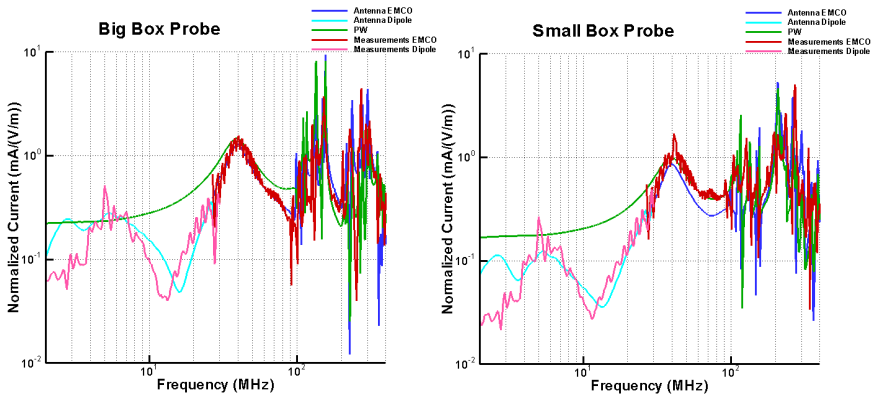
Figure 5. EMCO antenna, dipole antenna, and plane-wave (PW). Experimental vs. numerical comparison.

where data from the simulation with the antennas, plane-wave, and measurements have been put together. As stated above, these figures reveal a good capture of the peaks illuminating with a plane-wave over 30 MHz (EMCO frequencies). Below 30 MHz (dipoles' frequencies) the plane-wave approximation does not provide results consistent with measurements.

In conclusion, the plane-wave model permits further experimental testing for different angles, polarizations, etc. to be replaced by numerical experiments, which is required for certification. It bears noting that even for the low-frequency range a plane-wave excitation can be more realistic than the dipole antenna one, since it is closer to real flight conditions. However, just for validation purposes, the antenna model needs to be considered for the low-frequency band.

3.3. Object Rotation

In this section the sensitivity to different illumination angles is analyzed. It is always difficult to keep this parameter completely under control in the test setup, while effects due to this issue can be easily assessed by simulation.

For this analysis, let us start from the original EMCO antenna model, including the platform floor. The currents induced with the original EUT have been compared with the ones obtained with the EUT tilted 5 degrees around the vertical axis.

The comparison between numerical data for 0 and 5 degrees, and the measurements supposed to be in 0 degrees can be seen in Fig. 6.
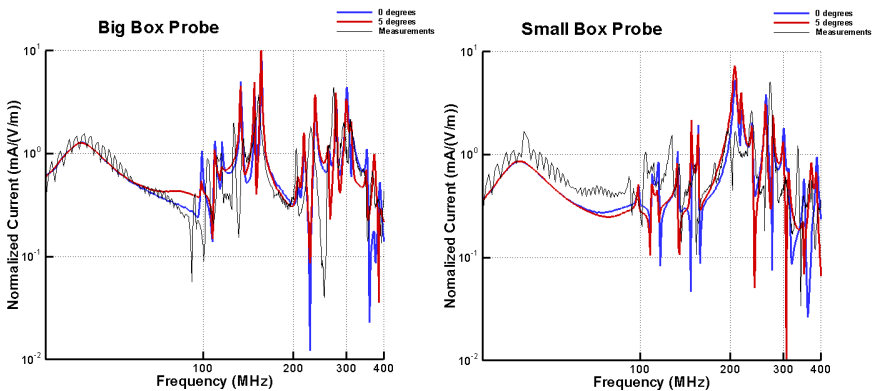
Figure 6. Rotation of the EUT by 5 degrees. Comparison with untilted original data.

The induced currents change slightly, and the differences are within the order of the numerical and measurement differences found throughout this study, providing us a criterion to interpret the numerical results in terms of the uncertainty of the experimental setup.

Let us stress here again that, after validation of the model, for certification purposes, a battery of numerical simulations should be performed including any of these setup changes, in order to determine the worst case.

3.4. Shifting the Probe Position

In this paragraph the influence of the probe location is studied, by using the simplified model with the plane-wave illumination (no platform floor). We have considered several Ampere-loop probes around the cable at different positions along it, shifted from the original experimental location. Numerical results serve to reflect the importance of placing the probe at exactly the same point as during the tests.

For the big box, 10 probes have been used: 9 of them separated 2 FDTD cells (13 mm), and the last one a bit more separated. Fig. 7(a) shows the comparison between the induced currents measured by these probes. The deviation is very slight at lower frequencies and only somewhat greater at higher frequencies. In any case, the deviation observed is the amplitude of the peaks, but not the frequency of the resonances. The last probe exhibits a larger difference because it is more separated than the other probes.

For the small box, we have used 10 probes separated by 4 FDTD

(a)   (b)
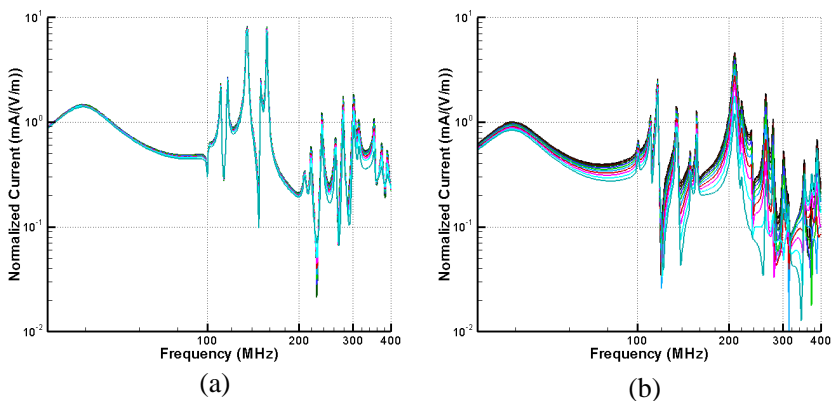
Figure 7. Current for different locations of the probes.

cells (26 mm) each one. Fig. 7(b) the comparison between the induced currents measured by these 10 probes. Again, we find differences in the amplitude of the peaks (not in their location), which may be important, especially at higher frequencies. Notice that the separation between the first and the last probe is $234\,\text{mm} \simeq \lambda/4$ at $300\,\text{MHz}$, which cannot be neglected in terms of position of peaks and nulls due to cable resonances over this frequency (a peak in a position can become a minimum, and so on).

In conclusion, the probe location must be kept under control (in terms of electrical size) for validation, especially for higher frequencies. However, for certification proposes, the simulation data found from several probe positions must be used in order to estimate the worst case.

4. CONCLUSIONS

In this paper, we have exemplified the construction of a reduced model, for the numerical simulation with FDTD of a cable harness under HIRF conditions, for which experimental data are available.

Performing HIRF measurements is not an easy task, and many test uncertainties must be under control and considered in the simulation model and/or approach, while other uncertainties can be neglected with no impact. While this task is part of the expertise of an engineer, some general conclusions can be drawn.

In the case presented, we have been able to use the experimental data to find and validate a computationally affordable numerical test setup, taking into account that, in general:

(i) Antennas can be removed from the numerical setup if they are in the far-field regime. However, in the near-field, the antenna should be considered in the model in order to make comparisons with measurements.

(ii) Non-relevant elements (for our GO31 case, the platform floor) can be carefully removed, assuming that there is a calibration phase, and that the observables are normalized by the calibration field.

The validated simplified final setup can be successfully used for certification purposes, employing only simulation, with the subsequent saving in experimental effort. Changes in antenna position, probe position, etc. can be made only in the numerical model to find the worst possible level of current sought in the certification process. For our GO31 test case, we can state that:

(i) The use of the plane-wave over the whole frequency range can be even more realistic under flight conditions than the experimental

conditions. It permits the reduction in the computational domain and the reuse of the same mesh for all the scenarios under analysis.

(ii) Several probe positions can be analyzed in a single simulation to select the worst case among all of them.

ACKNOWLEDGMENT

REFERENCES

1. Zhao, X.-W., X.-J. Dang, Y. Zhang, and C.-H. Liang, "The multilevel fast multipole algorithm for EMC analysis of multiple antennas on electrically large platforms," *Progress In Electromagnetics Research*, Vol. 69, 161–176, 2007.

2. Ali, M. and S. Sanyal, "A numerical investigation of finite ground planes and reflector effects on monopole antenna factor using FDTD technique," *Journal of Electromagnetic Waves and Applications*, Vol. 21, No. 10, 1379–1392, 2007.

3. Lei, J.-Z., C.-H. Liang, W. Ding, and Y. Zhang, "EMC analysis of antennas mounted on electrically large platforms with parallel FDTD method," *Progress In Electromagnetics Research*, Vol. 84, 205–220, 2008.

4. Lei, J. Z., C. H. Liang, and Y. Zhang, "Study on shielding effectiveness of metallic cavities with apertures by combining parallel FDTD method with windowing technique," *Progress In Electromagnetics Research*, Vol. 74, 85–112, 2007.

5. Yee, K., "Numerical solution of initial boundary value problems involving Maxwell's equations in isotropic media," *IEEE Transactions on Antennas and Propagation*, Vol. 14, No. 3, 302–307, 1966.

6. Taflove, A. and S. Hagness, *Computational Electrodynamics: The Finite-difference Time-domain Method,* 3rd Edition, Artech House, Boston, MA, 2005.

7. Garcia, S. G., A. R. Bretones, B. G. Olmedo, and R. G. Martín, "Finite difference time domain methods," *Time Domain Techniques in Computational Electromagnetics*, D. Poljak (ed.), 91–132, WIT Press, 2003.

8. Garcia, S. G., A. R. Bretones, B. G. Olmedo, and R. G. Martín, "New trends in FDTD methods in computational electrodynamics: Unconditionally stable schemes," *Recent Res. Development in Electronics*, Transworld Research Network, 2005.

9. Berenger, J.-P., "A perfectly matched layer for the absorption of electromagnetic waves," *Journal of Computational Physics*, Vol. 114, No. 1, 185–200, 1994.

10. [Online] Available: http:://www.hirf-se.eu.

11. *The Certification Of Aircraft Electrical And Electronic Systems For Operation In The High-intensity Radiated Fields (hirf) Environment*, Federal Aviation Administration Std. AC No: 20–158, Jul. 2007.

12. *Guide to Certification of Aircraft in a High Intensity Radiated Field (HIRF) Environment*, EUROCAE Std., Rev. EUROCAE ED-107, March 2001/SAE ARP 5583, Rev. A, Jun. 2010.

13. Georgakopoulos, A. V., C. R. Birtcher, and C. A. Balanis, "HIRF penetration through apertures: FDTD versus measurements," *IEEE Transactions on Electromagnetic Compatibility*, Vol. 43, No. 3, 282–294, Aug. 2001.

14. http://www.ugrfdtd.es.

15. [Online] Available: http://www.airbusmilitary.com/A330MRTT. aspx.

16. Berenger, J.-P., "A multiwire formalism for the FDTD method," *IEEE Transactions on Electromagnetic Compatibility*, Vol. 42, No. 3, 257–264, 2000.

17. Guiffaut, C., A. Reineix, and B. Pecqueux, "New oblique thin wire formalism in the FDTD method with multiwire junctions," *IEEE Transactions on Antennas and Propagation*, No. 99, 2011, early Access.

18. Balanis, C. A., *Advanced Engineering Electromagnetics,* John Wiley, 1989.